

Intracerebral Injection of Graphene Oxide Nanosheets Mitigates Microglial Activation Without Inducing Acute Neurotoxicity: A Pilot Comparison to Other Nanomaterials

Corinne Portioli, Cyrill Bussy,* Mariarosa Mazza, Neus Lozano, Dhifaf A. Jasim, Maurizio Prato, Alberto Bianco, Marina Bentivoglio, and Kostas Kostarelos*

Carbon-based nanomaterials (CNMs) are being explored for neurological applications. However, systematic *in vivo* studies investigating the effects of CNM nanocarriers in the brain and how brain cells respond to such nanomaterials are scarce. To address this, functionalized multiwalled carbon nanotubes and graphene oxide (GO) sheets are injected in mice brain and compared with charged liposomes. The induction of acute neuroinflammatory and neurotoxic effects locally and in brain structures distant from the injection site are assessed up to 1 week postadministration. While significant neuronal cell loss and sustained microglial cell activation are observed after injection of cationic liposomes, none of the tested CNMs induces either neurodegeneration or microglial activation. Among the candidate nanocarriers tested, GO sheets appear to elicit the least deleterious neuroinflammatory profile. At molecular level, GO induces moderate activation of proinflammatory markers compared to vehicle control. At histological level, brain response to GO is lower than after vehicle control injection, suggesting some capacity for GO to reduce the impact of stereotactic injection on brain. While these findings are encouraging and valuable in the selection and design of nanomaterial-based brain delivery systems, they warrant further investigations to better understand the mechanisms underlying GO immunomodulatory properties in brain.

1. Introduction

Nanomaterials may offer new solutions for unmet medical needs in the treatment of neurological disorders.^[1–4] Among the different types of nanomaterials suitable for these biomedical applications, carbon-based nanomaterials (CNMs), including single-walled (SWNTs) or multiwalled carbon nanotubes (MWNTs) and graphene have recently emerged as potential new candidates given their remarkable interaction with the neural tissue.^[5–10] CNMs possess unique physicochemical properties, such as high surface area, mechanical strength, electrical conductivity,^[11–15] and the ability to be chemically functionalized.^[16,17] In the context of neuroscience, these properties have been shown to support neuronal activity^[17] and facilitate drug delivery in the brain.^[18,19]

Studies performed *in vitro* have for instance revealed the promising applications of functionalized SWNTs as


Dr. C. Portioli, Dr. C. Bussy, Dr. M. Mazza, Dr. N. Lozano, Dr. D. A. Jasim, Prof. K. Kostarelos

Nanomedicine Lab
School of Health Sciences
Faculty of Biology, Medicine and Health
The University of Manchester
Manchester M13 9PL, UK
E-mail: cyrill.bussy@manchester.ac.uk;
kostas.kostarelos@manchester.ac.uk

Dr. C. Portioli, Dr. M. Bentivoglio
Department of Neurosciences
Biomedicine and Movement Sciences
University of Verona
Verona 37134, Italy

Dr. C. Bussy, Dr. N. Lozano, Dr. D. A. Jasim, Prof. K. Kostarelos
National Graphene Institute
The University of Manchester
Manchester M13 9PL, UK

Dr. C. Bussy
Lydia Becker Institute of Immunology and Inflammation
Faculty of Biology, Medicine and Health
The University of Manchester
Manchester M13 9PL, UK

 The ORCID identification number(s) for the author(s) of this article can be found under <https://doi.org/10.1002/smll.202004029>.

DOI: 10.1002/smll.202004029

Prof. M. Prato
Department of Chemical and Pharmaceutical Sciences
University of Trieste
Trieste 34127, Italy

Prof. M. Prato
Center for Cooperative Research in Biomaterials (CIC biomaGUNE)
Basque Research and Technology Alliance (BRTA)
Paseo de Miramón 182, Donostia-San Sebastián 20014, Spain

Prof. M. Prato
Ikerbasque, Basque Foundation for Science
Bilbao 48009, Spain

Dr. A. Bianco
CNRS
Immunology, Immunopathology and Therapeutic Chemistry
UPR3572, ISIS
University of Strasbourg
Strasbourg 67000, France

Dr. N. Lozano, Prof. K. Kostarelos
Catalan Institute of Nanoscience and Nanotechnology (ICN2)
and The Barcelona Institute of Science and Technology (BIST)
Campus UAB, Bellaterra, Barcelona 08193, Spain

glutamate uptake enhancers in primary astrocytes^[20] or as neuroprotective factors in primary glial cells extracted from brains of an Alzheimer's disease (AD) mouse model.^[21] Similarly, in animal models, functionalized CNMs were efficient in delivering siRNA in a stroke model^[22] or as drug carrier in an AD model.^[23] Another step toward their clinical translation was achieved when the translocation of functionalized MWNTs (f-MWNTs) across the blood–brain barrier (BBB) was demonstrated, initially *in vitro*^[24,25] and then *in vivo*.^[26,27] These seminal studies have paved the way toward the targeted delivery of active therapeutics across the BBB after peripheral administration of CNMs, as proposed in one proof-of-concept *in vivo* study for brain glioma.^[19] More recently, graphene-based materials (GBMs) and in particular graphene oxide (GO), the oxidized form of graphene that results from chemical exfoliation of graphite, have also been explored for brain therapy.^[6,15] Noticeably, GBMs were shown to inhibit the formation of β -amyloid aggregates and could thus be beneficial in preventing the progression of AD.^[28] Then, chemically functionalized GO sheets were reported to be suitable photothermal platforms for destroying formed amyloid aggregates in AD model upon near-infrared light irradiation, via the generation of localized heat.^[29,30] Finally, GBMs were used as nanocarriers for antitumor drugs in both *in vitro* and *in vivo* models of brain cancer,^[18,31] and as neurotransmission modulator with potential applications in neurobiology.^[32]

However, a key issue for a more widespread use of nanocarriers (including CNMs) in brain therapy is the response of the brain parenchyma once nanomaterials interact with the different cell populations of the central nervous system (CNS). This becomes especially crucial in view of potential applications of nanocarriers in brain diseases with an inherent neuro-inflammatory component, such as neurodegeneration, stroke, infection, or cancer.^[33–35] Therefore, to support the exploration of the full potential of CNMs for brain therapy applications, increasing effort has been devoted to investigate the possible side effects of these materials upon interaction with the brain parenchyma. MWNTs coated with polymeric material (Pluronic F127, used to increase solubility of MWNTs) were initially incubated with primary cortical neurons.^[36] As these MWNTs did not induce apoptotic effects *in vitro*, their biocompatibility was then validated *in vivo* upon injection in the visual cortex of mice.^[36] Similarly, no major tissue damages were reported in another study performed to analyze the neuroinflammation and cellular uptake of two types of f-MWNTs (carboxylated or amino-functionalized), after injection in the cerebral cortex.^[37] Both f-MWNT types were internalized by microglial cells and neurons, and elicited a higher glial cell marker expression at the injection site, 2 days after injection.^[37] However, at 30 days postinjection, only carboxylated MWNTs resulted in persistent glial cell activation in regions peripheral to the injection site.^[37] In another set of studies, after the infusion of PEGylated SWNTs in the hippocampus of rats, an antioxidant response was observed after 24 h^[38] and up to 7 days.^[39] The authors theorized that the antioxidant response to SWCNTs could partly explain the moderate impact of the nanomaterials on animal behaviors;^[38] moreover, the biopersistence of these CNMs at the injection site was ascribed for the persistence of the antioxidant response over 7 days.^[39] Lastly, a study on the neurotoxic effect of different f-MWNTs using primary cultures of neuronal

and glial cells derived from either the striatum or frontal cortex revealed that while f-MWNTs did not affect neuronal cells from any of the two brain regions or glial cells from the frontal cortex, the viability of striatum-derived glial cells decreased.^[40] Although the brain region-dependent cytotoxicity to glial cells was shown to be independent of the f-MWNT type, it was instead associated with the number of microglial cells in the considered brain region-derived cell cultures,^[40] highlighting the key role of microglial cells (the resident macrophages of the brain) in the regulation of the biological response to CNMs.

More recently, the potential impact of GBMs on brain cells and tissue has also been explored. Functionalized graphene-based systems investigated as drug delivery carriers in the treatment of subarachnoid hemorrhage did not show neurotoxicity in the targeted region.^[41] However, GO sheets were reported to down-regulate neuronal activity and signaling *in vitro*, albeit without affecting viability.^[42,43] Autophagy and calcium homeostasis were also found to be disturbed in neuron cultures exposed to GO, highlighting the ability of GO sheets to damage neuronal transmission and functionality, without inducing toxicity.^[43] Astrocyte function and homeostasis were similarly altered by GO sheet exposure and internalization, subsequently impacting the neuronal network that astrocytes were supporting.^[44] Finally, when primary mixed glia or the microglia BV2 cell line were pretreated with GO sheets, inhibition of NLRP3 inflammasome-dependent interleukin (IL)-1 β secretion was observed upon lipopolysaccharide (LPS) and ATP priming.^[45]

Despite this growing knowledge and the great potential of CNMs as brain drug delivery vectors, systematic studies assessing the inflammatory potential of these nanocarriers in brain tissue remain scarce. To address this gap, three different types of engineered CNMs, including one GO type and two f-MWNTs (aminated or carboxylated), were here injected stereotactically into the striatum of mice and their potent inflammation was assessed. For comparison, two types of highly charged liposomes were used as benchmark drug delivery systems with previously reported tissue^[46,47] and brain^[48,49] inflammogenicity. Considering recent findings highlighting the immunomodulatory and anti-inflammatory properties of GO sheets *in vitro* and *in vivo*,^[32,45,50] the present study was also designed to test the hypothesis that GO materials present a unique inflammation profile when compared to other nanomaterials. The inflammatory potential of the different candidate nanocarriers was therefore assessed at different time points of the acute early stage response (up to 1 week after injection) at both the molecular (i.e., transcripts encoding a panel of cytokines and chemokines) and histological (i.e., activation of astrocytes and microglial cells, number of neurons and dead cells) levels. These analyses were performed not only at the injection site (central position in the striatum) but also in adjacent and distant positions within the brain, to assess both the diffusion of inflammation processes and the delocalized effects caused by nanomaterial diffusion.

2. Results

2.1. Characterization of the NMs

Either aminated or carboxylated f-MWNTs that have been previously explored for biomedical applications were used in the

present study.^[22,37,51–54] Their chemical functionalization is thought to not only improve solubility, but also increase biocompatibility by reducing toxicity through mitigation of the material–cell membrane interaction. The dimensional features (diameter and length) of those f-MWNTs were analyzed by transmission electron microscopy (TEM; **Figure 1B**; **Figure S1A**,

Supporting Information). Both types of f-MWNTs had an outer diameter between 20 and 30 nm. Carboxylated f-MWCNTs (ox-MWNTs) were between 200 and 300 nm in length, while aminated f-MWNTs (MWNT-NH₃⁺) had a length between 500 and 2000 nm. The Kaiser test was performed to establish the amount of amino groups present on the MWNT-NH₃⁺, and a

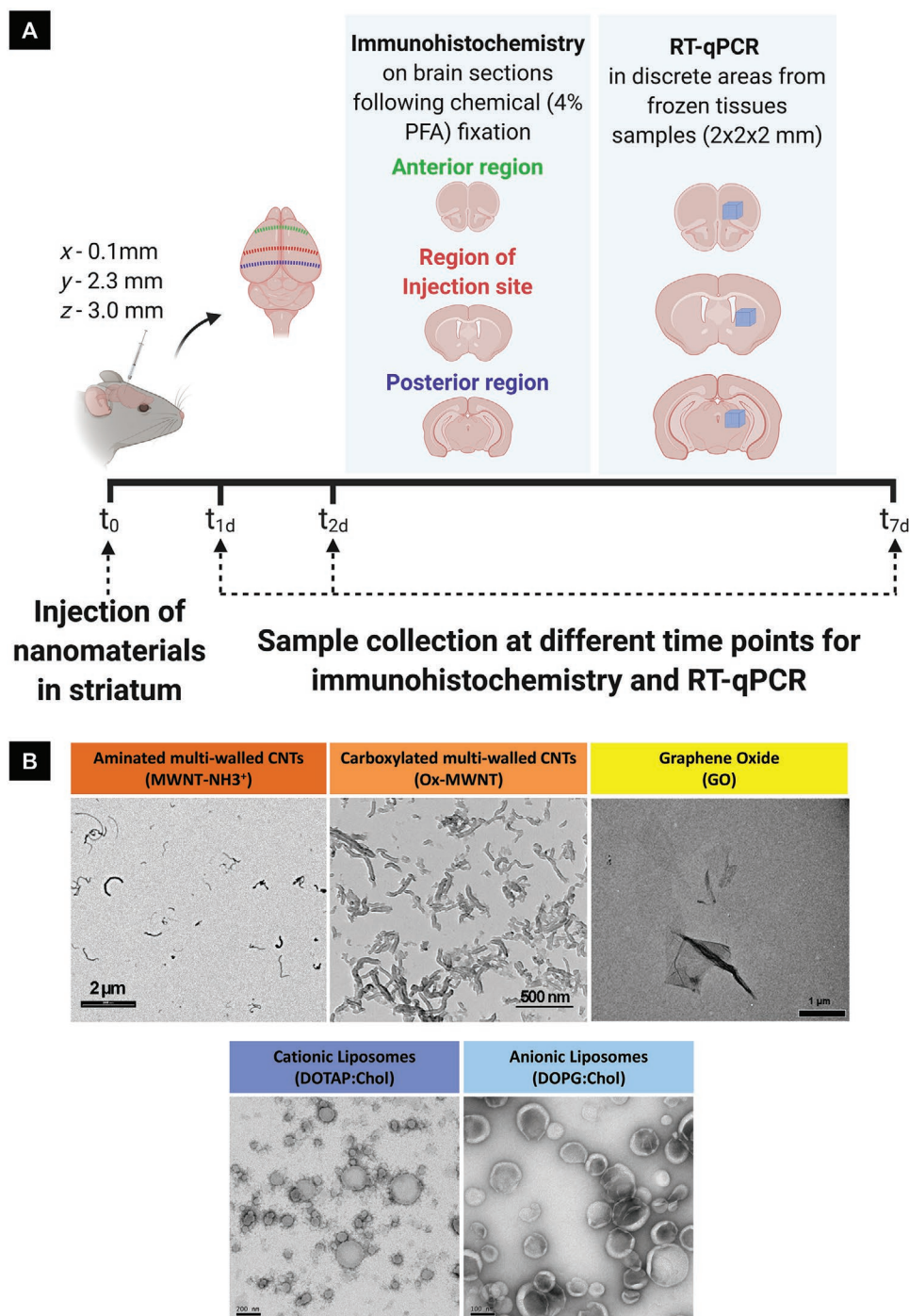


Figure 1. Experimental design scheme and TEM of the different nanomaterials tested. A) Experimental design of the present study. After stereotactic administration of different nanomaterials, brains were collected at different time points. Molecular and cellular analyses were performed in the injection site and in nearby regions (anterior and posterior). B) Transmission electron microscopy characterization of the nanomaterials (aminated MWNTs, carboxylated MWNTs, GO, and cationic and anionic liposomes) used in this work.

loading of 58 $\mu\text{mol g}^{-1}$ of amino functional groups was found (Figure S1A, Supporting Information); while the amount of carboxyl group on the ox-MWNTs had been previously determined using thermogravimetric analysis and a loading of 1.7 $\mu\text{mol g}^{-1}$ was found.^[55]

In line with our previous works, several techniques were used to assess the physicochemical properties of GO sheets (Figure 1B; Figure S1B, Supporting Information). The ζ -potential was -50.0 ± 0.4 mV. The lateral dimensions were established with TEM and were in between 10 and 1800 nm, while atomic force microscopy (AFM) revealed a thickness between 0.9 and 4.8 nm, consistent with few layer 2D materials, as we previously reported.^[56,57]

Characterization of cationic (1,2-dioleoyl-3-trimethylammonium-propane hydrochloride (DOTAP):cholesterol (Chol)) and anionic (1,2-dioleoyl-sn-glycero-3-[phospho-rac-(3-lysyl(1-glycerol))]) (DOPG):Chol liposomes was performed to confirm their hydrodynamic diameter size, polydispersity index (PDI) and ζ -potential (Figure 1B; Figure S1C, Supporting Information). Cationic (DOTAP:Chol) and anionic (DOPG:Chol) liposomes showed a hydrodynamic diameter of 125.6 ± 2.6 nm and 118.1 ± 3.0 nm, respectively. DOTAP:Chol liposomes showed a PDI of 0.254 ± 0.004 , while in the case of DOPG:Chol liposomes, the PDI was 0.393 ± 0.061 . The surface charge of the liposomes was confirmed by ζ -potential measurements. DOTAP:Chol liposomes were formed by positively charged polar chains (DOTAP; Figure S1C, Supporting Information) that attribute the cationic nature to the system ($\zeta = +60.5 \pm 2.6$ mV), while DOPG:Chol liposomes were formed by negatively charged polar chains (DOPG; Figure S1C, Supporting Information) that attribute the anionic nature to the system ($\zeta = -54.1 \pm 0.5$ mV).

2.2. Expression of Inflammation-Related Genes

The gene expression levels of transcripts encoding inflammatory molecules were measured in the sampled brain tissue blocks. Transcripts encoding TNF- α , IL-1 β , IFN- γ , IL-6, and IL-12 were used to evaluate proinflammatory cytokines, CCL2 and CXCL10 as proinflammatory chemokines, and IL-10, IL-4, and TGF- β as anti-inflammatory markers (Table S1, Supporting Information).

2.2.1. Central Brain Injection Site

The gene expression results for inflammatory markers in the injection site (central striatum) are presented in Figure 2. As expected, bacterial LPS injection (positive inflammation control) induced significantly higher expression levels for all inflammatory transcripts tested, except for *ifn- γ* mRNA at day 1 and *cxcl10* mRNA at day 1 and day 2. At day 7, the upregulation of inflammatory transcripts induced by LPS was lower than at the two shorter time points, but remained significantly different from *il-10* mRNA induced by dextrose injection. Surprisingly, there was no significant upregulation of *cxcl10* expression at any time point.

In contrast, carbon nanomaterials had a limited effect on the expression levels of these genes (Figure 2). Over time, ox-MWNTs had a limited impact at day 1 (upregulation of *tnf- α*

and *il-1 β* mRNAs), high impact at day 2 (upregulation of *il-12*, *ifn- γ* , *il-6*, and *tgf- β* mRNAs), and returned to basal levels at day 7. Similarly, GO upregulated only *tgf- β* expression at day 1, upregulated *tnf- α* and *il-6* expression at day 2, but had no effect at day 7. MWNT-NH₃⁺ upregulated only the *il-6* gene at both day 1 and day 2 but had no effect at day 7. Comparison of the three carbon NMs revealed that MWNT-NH₃⁺ had the safest inflammatory profile at day 1 while GO was the safest at day 7. At day 2, both MWNT-NH₃⁺ and GO behaved similarly, while ox-MWNTs induced the greatest inflammation.

Liposomes were used here as positive nanomaterial controls and were found to more broadly affect gene expression (Figure 2). DOTAP:Chol upregulated *il-6* and *il-10* mRNAs at day 1; this upregulation persisted at day 2, when expression levels of *tnf- α* , *il-1 β* , and *tgf- β* mRNAs were also upregulated. In addition, the inflammation induced by DOTAP:Chol was maintained at day 7 with upregulation of *ifn- γ* , *ccl2*, and *cxcl10* gene transcripts. Similarly, DOPG:Chol upregulated *il-12*, *il-6*, and *il-10* mRNAs at day 1 and upregulated *tnf- α* , *il-1 β* , *il-12*, *il-10*, and *ccl2* expression at day 2 but returned to basal level at day 7. When comparing the two types of liposomes, no significant differences were observed for any inflammatory marker at day 1. At day 2, significant differences were found for *ccl2* mRNA only. At day 7, significant differences were found for *tnf- α* , *ifn- γ* , *il-12*, *ccl2*, and *cxcl10* mRNAs, revealing an accentuated proinflammatory profile for cationic DOTAP:Chol liposomes in comparison to anionic DOPG:Chol liposomes.

Among the different NMs, carbon NMs appeared to elicit the mildest inflammatory response at the injection site. Both MWNT-NH₃⁺ and GO yielded similar results, whereas ox-MWNT was the most proinflammatory NM, especially at day 1 and day 2 postinjection.

2.2.2. Adjacent Posterior Brain Region

The results of gene expression for different inflammatory markers in the posterior brain region in direct contact with the injection site are presented in Figure S2 in the Supporting Information. After LPS injection, upregulation of transcript levels for all markers followed the same trends as in the site of injection. At day 1 and day 2, all transcripts were upregulated except for *ifn- γ* mRNA at day 1. At day 7, expression of the *tnf- α* and *il-1 β* genes were still upregulated.

At day 1, carbon NMs had no significant impact on the expression of any of the genes tested in this brain region (Figure S2, Supporting Information). At day 2, all three carbon NMs regardless of their characteristics significantly downregulated *tnf- α* expression and upregulated *ccl2* expression. At day 7, none of the carbon NMs had any significant effect. No significant differences were observed at any time point among the three carbon NMs, despite a trend suggesting a mild (compared to nanotubes) inflammatory profile after GO administration, especially at day 7 (i.e., *ccl2*, *il-12*, and *ifn- γ* mRNAs had lower values, albeit without statistical significance).

In contrast, following injection of liposomes, DOPG:Chol significantly upregulated *ccl2* and *cxcl10* mRNAs at day 1, whereas DOTAP:Chol had no effect in the posterior brain region (Figure S2, Supporting Information). At day 2, while

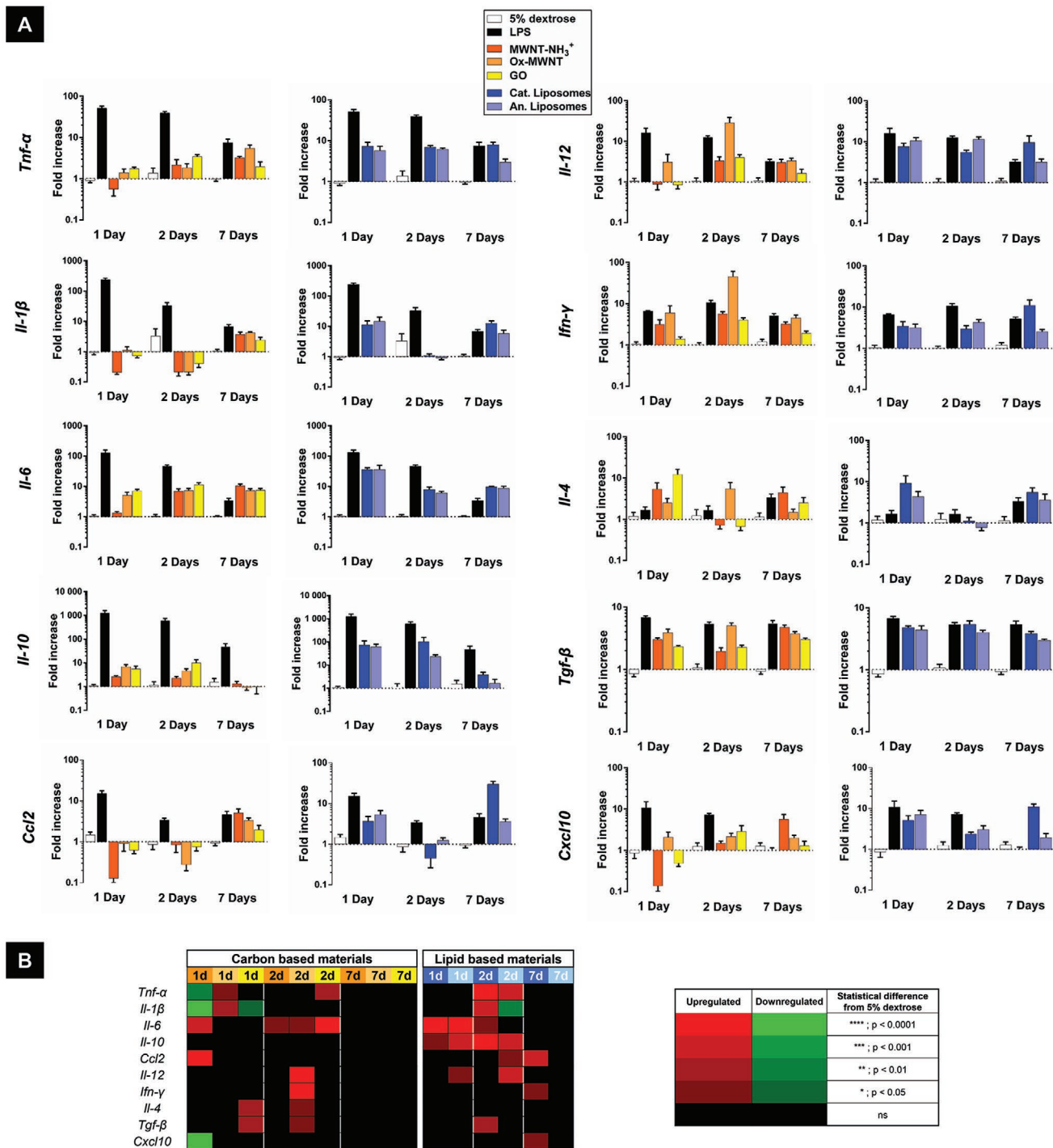


Figure 2. RT-qPCR analysis results obtained in the brain striatum injection site. A) Gene expression levels of transcripts encoding proinflammatory cytokines, chemokines, and anti-inflammatory cytokines. The analysis was performed at 1, 2, and 7 days after injection of LPS, 5% dextrose, cationic or anionic liposomes (1 $\mu\text{g } \mu\text{L}^{-1}$), MWNT-NH₃⁺ or ox-MWNT (0.5 $\mu\text{g } \mu\text{L}^{-1}$), or GO (0.5 $\mu\text{g } \mu\text{L}^{-1}$). B) Heatmap presenting the statistical analysis. All statistical differences are shown in heatmap colors comparing dextrose with all types of material injected. Mean \pm SEM, * $p < 0.05$, ** $p < 0.01$, *** $p < 0.001$, and **** $p < 0.0001$ versus 5% dextrose.

DOTAP:Chol significantly upregulated *il-1β* and *il-10* transcripts, DOPG:Chol upregulated *tnf-α* and *ccl2* mRNAs. At day 7, none of the liposomes had any effect on inflammatory

marker gene expression, highlighting the transient inflammatory impact of these materials, possibly due to their well-known poor long-term structural stability in living tissue.

2.2.3. Distant Anterior Brain Region

Gene expression levels for the inflammatory markers in the anterior brain region (distant from the injection site) are presented in Figure S3 in the Supporting Information. As described above, at day 7 in the posterior brain region (in direct contact with the injection site), a drastic decrease of the inflammatory response for all markers and conditions tested was observed, including LPS injection (Figure S2, Supporting Information). We therefore reasoned that in a distant brain site (not in direct contact with the site of injection) inflammation levels at day 7 would be even lower. This led us to investigate gene transcripts in the distant anterior brain region only at day 1 and day 2 (Figure S3, Supporting Information). A second motivation for performing analyses of gene transcripts in the anterior striatum after injection in the middle/central striatum (these two parts of the striatum being at relative distance from each other) was brought about the hypothesis that liposomes can diffuse across this brain region and therefore induce inflammation beyond the site of injection.^[58,59] In addition, analyses were performed only for liposomes, as they were inducing upregulation of genes in the posterior brain region (Figure S2, Supporting Information), whereas all carbon NMs did not induce any gene upregulation in this brain region (Figure S2, Supporting Information).

The results following LPS injection in the anterior brain region were identical to those found for the posterior brain region at day 1 and day 2, with an upregulation of all markers except for *ifn-γ* expression at day 1 (Figure S3, Supporting Information). At day 1, anionic DOPG:Chol liposomes elicited the greatest inflammatory response, with significant upregulation of *tnf-α*, *il-1β*, *il-6*, *ccl2*, and *cxcl10* mRNAs, whereas cationic DOTAP:Chol only upregulated *il-1β* expression. In contrast, DOTAP:Chol liposomes were more inflammatory at day 2, with upregulation of *tnf-α*, *il-1β*, *ccl2*, and *cxcl10* expression, while DOPG:Chol liposomes only upregulated *il-12* expression.

Overall, anionic DOPG:Chol liposomes seemed to have a greater inflammatory potential at day 1 and day 2 not only at the injection site but also in nearby and distant regions of the brain. In contrast, cationic DOTAP:Chol liposomes showed a greater inflammatory potential at day 2 in all brain regions, persisting at day 7 only in the site of injection. These results suggested that liposomes, as hypothesized, can diffuse across the brain tissue from the injection site and mediate proinflammatory effects along their path.

2.3. Impact on Microglial Cells and Astrocytes

To investigate the effect of the tested NMs on microglial cells and astrocytes, we focused our efforts on day 2. This time point was selected based on the molecular findings presented above, which indicates that expression levels of proinflammatory transcripts were higher 2 days after injection than at the other time points. The same three brain regions assessed for the RT-qPCR analyses were used for the histology study (Figure 1A).

Glial cell analyses were based on CD11b and glial fibrillary acidic protein (GFAP) immunophenotyping. Both qualitative observations of cell features to detect structural changes

indicating an activated state (such as cell body hypertrophy and increased thickness of processes) and quantitative analyses were performed (CD11b; Figure 3A-i,B-i,C-i; GFAP, Figure 3A-ii,B-ii,C-ii). The latter evaluated the following different parameters: i) area covered by microglia and astrocytes, including cell branches (a higher area indicating cell hypertrophy) (Figures S4A and S5A, Supporting Information), ii) intensity of microglial cell immunoreactivity evaluated by densitometry (increased intensity indicating CD11b upregulation) (Figure S4B, Supporting Information), and iii) astrocyte cell number (an increased cell number indicates astrocytic activation) (Figure S5B, Supporting Information).

The area covered by microglial cells (Figure 3A-i,B-i,C-i) and astrocytes (Figure 3A-ii,B-ii,C-ii) was evaluated for all conditions tested and in the three brain regions considered. The analysis was also conducted in matched regions of the contralateral hemisphere to obtain data in tissue devoid of mechanical trauma due to stereotactic injection or surgery.

2.3.1. Microglial Cells

Immunolabeled microglial cells at the injection site did not show features of activation, or only mild activation in comparison to vehicle control (5% dextrose in water), at day 2 after injection (Figure S4A, Supporting Information; Figure 3B-i). This was observed for all NMs and doses tested here. Only injection of cationic DOTAP:Chol or anionic DOPG:Chol liposomes replicated the features observed after LPS injection (i.e., hypertrophy and “bushy” appearance of microglial cells). However, this was not significantly different from the vehicle control, as analyzed quantitatively (Figure 3B-i). High cell death, likely involving both neurons and glia, was observed at the site of injection after either of these liposomal treatments and could account for this finding. Surprisingly, GO injections at 1 mg mL⁻¹ resulted in significantly lower CD11b immunoreactivity than control vehicle injection and was similar to that observed in the contralateral noninjected hemisphere (Figure 3B-i). Administration of either type of f-MWNTs at both 0.5 and 1 mg mL⁻¹ and GO at 0.5 mg mL⁻¹ induced a glial cell activation comparable to that observed after vehicle injection.

In brain tissue sections distant from the injection site (i.e., anterior brain region), weak microglial cell activation was observed after NM injections, while LPS induced clear microglial cell activation (Figure S4A, Supporting Information). When analyzed quantitatively and in comparison to the contralateral region, only LPS injection elicited a significant activation of CD11b-positive cells (Figure 3A-i). All the other conditions, including both types of f-MWNTs or liposomes and GO, induced microglial cell activation at a level similar to that induced by vehicle injection or even lower, and was similar to that observed in the contralateral hemisphere. Only cationic DOTAP:Chol liposomes (and to a lesser extent DOPG:Chol liposomes) induced microglial cell activation that was slightly more pronounced (but not significant) than the vehicle.

In sections from brain tissue in direct contact with the injection site (i.e., posterior brain region), mild activation of microglial cells was observed after injection of LPS and anionic DOPG:Chol liposomes; this was also observed to

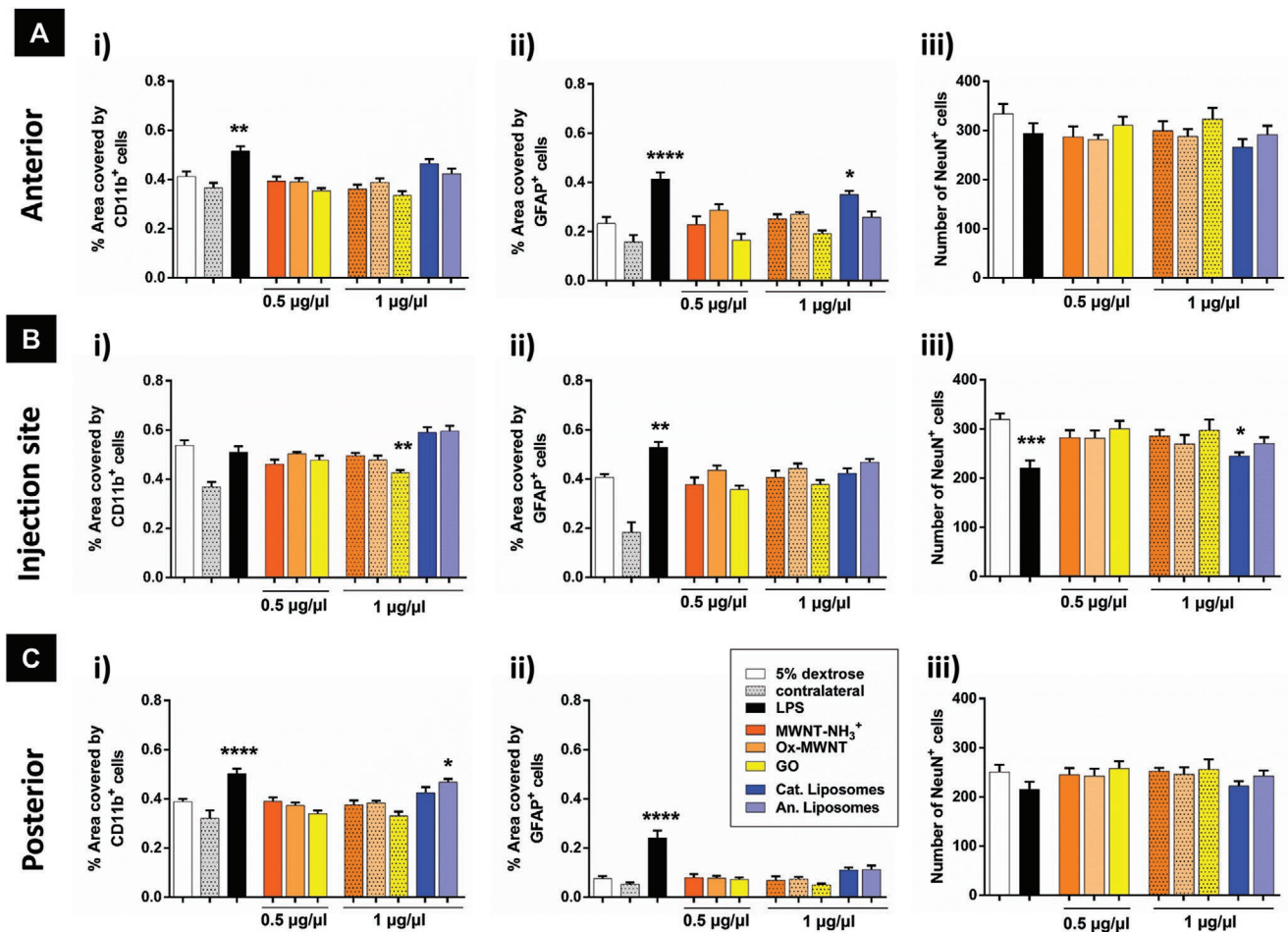


Figure 3. Quantitative analysis of glial cell immunohistochemical staining performed in different brain regions; A) anterior to the injection site, B) the injection site, and C) a posterior site nearby the injection site. i) Relative proportion of the area (mean per ROI) covered by microglial (CD11b-immunopositive) cells, or ii) astrocytes (GFAP-immunopositive cells) and iii) estimated number of neurons (NeuN-immunopositive cells) counted in ROI were performed in the site of injection and in the regions anterior and posterior 2 days after administration of LPS, 5% dextrose (ipsilateral and contralateral sides), MWNT-NH₃⁺ or ox-MWNT or GO (0.5 and 1 µg µL⁻¹), or cationic and anionic liposomes (1 µg µL⁻¹). Mean ± SEM; *p*-values are in comparison to 5% dextrose samples. **p* < 0.05, ***p* < 0.01, and *****p* < 0.0001 versus 5% dextrose. Representative images of the different immunostainings are presented in Figures S5–S7 in the Supporting Information.

a lesser extent after cationic DOTAP:Chol liposome injection (Figure S4A, Supporting Information). Accordingly, quantitative evaluation of the percentage of the area covered by CD11b-positive cells showed a significant increase only in brains after LPS or DOPG:Chol liposome injection (Figure 3C-i). DOTAP:Chol injection induced a modest, but not significant, increase of CD11b-positive cell coverage compared with both vehicle control injection and the contralateral region. Both types of f-MWNTs at either concentration had no effect on activation of microglial cells in this region with results similar to vehicle control injection. Noticeably, GO injection at either concentration resulted in a lower signal than the vehicle and was more comparable to the contralateral region, albeit not significantly.

Based on these results, particularly the surprising results obtained with GO versus liposomes or f-MWNTs, a densitometric evaluation of CD11b immunostaining intensity was performed in brain sections containing the injection site and

compared against results obtained from LPS- and vehicle-injected brain tissues (Figure S4B, Supporting Information). Consistent with the findings mentioned above, densitometric analysis revealed a significantly lower CD11b optical density after administration of GO than after vehicle, at the two tested GO doses. These results suggest that the presence of GO could be beneficial in reducing the trauma of surgical injection in the striatum. In contrast, and as expected, CD11b optical density after LPS injection was significantly higher than vehicle injection. Differences in this parameter between injection of DOTAP:Chol or DOPG:Chol liposomes and vehicle were not significant.

2.3.2. Astrocytes

Hypertrophic astrocytes, as indicated by higher GFAP immunoreactivity, were observed after LPS injection at the injection site

(Figure S5A, Supporting Information). Accordingly, the relative surface area covered by astrocytes after LPS injection showed a significant increase when compared with vehicle control injection (Figure 3B-ii). Although not significant, the area covered by GFAP-positive cells was also slightly increased after injection of ox-MWNT at both concentrations or injection of anionic DOPG:Chol liposomes when compared with vehicle. None of the other NMs induced significant differences when compared with vehicle control injections, but all conditions induced higher astrocyte coverage than in the matched, contralateral noninjected brain regions; this suggests that the mechanical trauma due to their respective injections could account for this mild astrocytic reaction.

In brain sections from the anterior region (distant from site of injection), mild features of astrocyte activation were observed after administration of LPS or cationic DOTAP:Chol liposomes (Figure S5A, Supporting Information). Accordingly, the relative surface area of the brain tissue covered by GFAP immunoreactivity was significantly higher after injection of LPS and DOTAP:Chol liposomes than after vehicle, although values were lower after injection of DOTAP:Chol than LPS (Figure 3A-ii). None of the other NMs induced significant differences. Although not significant, values were lower after GO injection than after vehicle injection (for both GO doses tested) and were similar to the contralateral hemisphere, consistent with the results for microglial cell reactivity after GO treatment. For all conditions, the relative surface area of the tissue covered by GFAP immunoreactivity was overall lower in this anterior brain region than at the injection site (Figure 3A-ii,B-ii).

In the posterior brain region (i.e., sections in close vicinity to the injection site), astrocyte activation was observed only after LPS injection and to a far lesser extent after DOTAP:Chol or DOPG:Chol liposome injection (Figure S5A, Supporting Information). Astrocytes had normal appearance for every other condition. These observations were supported by quantitative evaluation of the area covered by GFAP immunoreactivity (Figure 3C-ii). Only LPS induced a significant increase of GFAP coverage. Values after DOTAP:Chol or DOPG:Chol liposome injection were slightly higher than after vehicle administration, while every other condition showed values similar to or lower than vehicle-injected controls. Noticeably, values after GO at 1 mg mL⁻¹ were lower than after vehicle injection and similar to those in the matched contralateral brain region.

Considering these results and the higher astrocyte activation observed in the anterior brain region after injection of cationic DOTAP:Chol liposomes, astrocyte cell number was analyzed after injection of DOTAP:Chol liposomes and compared to both positive (LPS) and negative (vehicle) controls (Figure S5B, Supporting Information). DOTAP:Chol liposome injection did not significantly affect the number of astrocytes in the three analyzed brain regions, despite being higher than the vehicle control in the anterior brain region. The latter result was concordant with the relative coverage of GFAP-positive cells in DOTAP:Chol liposome-injected brains (Figure 3), which showed greater astrocyte activation than after vehicle injection but lower than after LPS injection. Astrocyte number was also significantly increased in the anterior and posterior brain regions after LPS injection, but was not significantly increased in the injection site. These findings were also in agreement

with the relative coverage of GFAP-positive cells that showed that LPS resulted in higher values in both the anterior and posterior brain regions (Figure 3A-ii,C-ii) than in the injection site (Figure 3E) when compared with vehicle. As mentioned above, this could be explained by the high cell death (involving glia) elicited by LPS in the injection site (Figure 3B-ii).

2.4. Impact on Neuronal Cell Viability

Akin to glial cells, the impact of the different NMs on neurons was also studied at day 2 after injection. Neuronal cell death following injection of NMs was quantified using NeuN immunostaining (Figure S6, Supporting Information). Statistical evaluation was performed by comparing each data set with that obtained after vehicle injection in the respective brain region (Figure 3A-iii,B-iii,C-iii). Only in the injection site and after LPS or cationic DOTAP:Chol liposome injections was a significant loss of neurons observed (Figure 3B-iii). LPS induced higher neuronal cell loss compared to DOTAP:Chol. No significant neuronal cell loss was observed after injection of the other NMs or in the other two brain regions.

Based on neuronal cell loss, the number of apoptotic cells were analyzed measuring the cleaved caspase 3 immunoreactivity after LPS and cationic DOTAP:Chol liposome injections, and were compared to vehicle and GO injections (Figure 4). The greatest number of cleaved caspase 3 positive cells was found in brain sections containing the injection site after LPS or cationic liposome injections, in agreement with the loss of NeuN immunoreactivity. Interestingly, a greater number of cleaved caspase 3 positive cells was also observed in the cerebral cortex at the level of the injection site, possibly associated with the needle track passing through the cortex to reach the

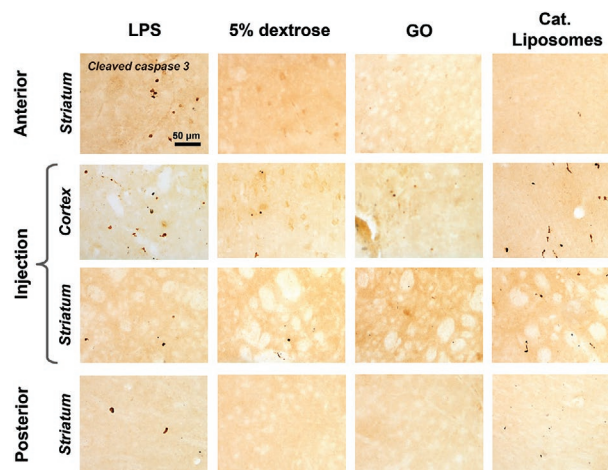


Figure 4. Representative images of cleaved-caspase 3 immunohistochemical staining. The immunophenotyping of cleaved-caspase 3 positive elements (undergoing apoptosis) in the injection site (the striatum), and in the anterior region distant from the injection site and in the posterior region adjacent to the injection site obtained at 2 days after injection of LPS, 5% dextrose, GO, and cationic liposomes. Note that apoptotic elements were visible in the injection site of LPS and cationic liposomes, while apoptotic cells visible in the GO-injected brain were comparable to the vehicle control (5% dextrose).

striatum, but only after LPS and DOTAP:Chol liposome injections and not after vehicle or GO injections. This suggests a safer toxicological profile for GO than DOTAP:Chol liposomes, consistent with the results obtained with CD11b immunoreactivity (Figure S3B, Supporting Information).

Finally, a Fluoro-Jade B staining was performed (Figure S7, Supporting Information) to label neurons undergoing degeneration.^[60] Combining Fluoro-Jade B staining with cleaved caspase 3 staining would help confirming whether cleaved caspase 3 positive cells were in fact neurons. Consistent with both the NeuN and cleaved caspase 3 signals, only LPS-injected brains had Fluoro-Jade B labeled neurons in the striatum. In the cortical tissue surrounding the needle track, a limited number of Fluoro-Jade B positive cells were observed after injection of LPS, DOTAP:Chol liposomes, or (to a lesser extent) vehicle. Surprisingly, no Fluoro-Jade B stained cells were observed after GO injection in the striatal or cortical regions, suggesting that the presence of GO sheets may have prevented the brain tissue damages associated to surgery and observed after vehicle injection, which supports the data obtained with CD11b immunoreactivity (Figure S4B, Supporting Information). Results from NeuN and cleaved caspase 3 immunostaining clearly revealed that NMs inducing neurotoxicity (i.e., DOTAP:Chol liposomes) were only detrimental at the site of injection, but not in adjacent brain regions. This finding was suggesting that, despite the potency of these materials to diffuse across the brain tissue (as indicated by their inflammatory potential across the three tested regions), the amount of diffusing materials is likely to be limited, or that neurotoxicity requires a high dose of materials, such as found at the injection site, to occur.

Taken together, the results obtained with NeuN, cleaved caspase 3 and Fluoro-Jade B indicate that only cationic DOTAP:Chol liposomes (and the positive control for inflammation, LPS) had a clear negative impact on cells and primarily at the site of injection. In contrast, GO appears to have a safer and potentially beneficial profile in respect to neurons.

3. Discussion

Due to their unique properties and dimensions, engineered nanomaterials have emerged as novel nanomedicine solutions for the treatment or diagnosis of various neurological conditions.^[1] However, the CNS is a very sensitive environment. If freely bioavailable in the brain parenchyma, nanosized foreign materials such as nanocarriers may easily cause disruption to physiological processes and functions. It is therefore of greatest importance that safety considerations are implemented at an early stage during the development of biomedical nanomaterials for CNS applications.^[61,62] For this to happen, a better understanding of the nanomaterial physicochemical characteristics that may induce adverse effects in the brain, such as inflammation, is warranted. This is particularly essential for biomedical nanomaterials developed to treat brain diseases that already have an inflammatory component.^[34,35]

Recently, both carbon nanotubes and graphene-based materials have shown great promise for the treatment and imaging of neurological disorders. However, there is a limited number of studies that have specifically explored the neuroinflammation

profiles of these CNMs in the brain. With this in mind, we went on investigating the neuroinflammatory potential of different CNMs that could potentially be used as brain nanomedicines. The tested nanocarriers were directly injected in the striatum, which was used here as a model of centrally positioned brain region for assessing the reactions of the three main cell types of the brain (namely, neurons, astrocytes, and microglial cells) to exogenous materials. Along with CNMs, both cationic and anionic liposomes were used as benchmark materials with known inflammatory properties in various tissues^[46,47] or the brain.^[48,49,63] These inflammatory properties are due to their high density of surface charges. Indeed, while anionic micelles were shown to be well tolerated regardless of administration modalities,^[48] cationic micelles and cationic liposomes elicited immune cell infiltration and neuronal degeneration due to inflammatory response after central administration.^[48,49]

In the present study, the inflammatory potential of the different nanomaterials was then tested at both molecular and histological levels. These investigations were performed not only in the area of the brain injected with the candidate nanocarriers, but also in adjacent brain areas, either in close vicinity to the site of injection (posterior area) or a few mm away from the site of injection (anterior area). This assessment in three different locations of the same striatum was designed to assess the possible diffusion of the materials or biological effects (or both) across the injected brain region, namely, the striatum. In addition, different doses of nanomaterials were considered. The main tested dose for f-MWNTs and GO (i.e., 0.5 μg) was based on previous studies for drug delivery purposes using similar administration route, bypassing the blood–brain barrier.^[22,53] This amount was then doubled to directly compare with the dose used for liposomes and to assess the role of positive and negative charges in the inflammation profile of surface-charged CNMs, such as functionalized MWNTs and GO. All tested materials were compared to a negative control, an injection with the vehicle (5% dextrose in water), which reflected the background inflammatory response to the brain tissue damage induced by the stereotactic surgical procedure. The reported neuroinflammation profiles for the different nanomaterials tested are therefore representing not only the brain tissue response to the material injections, but also how each tested nanomaterial modulated the inflammatory response inherent to the brain surgery used to administer those materials.^[50] NM treatments were also compared to LPS, a known inflammatory compound.

Gene expression analyses of pro- and anti-inflammatory markers revealed that the tested nanomaterials elicited different patterns of inflammatory response in the considered brain areas. In general, regardless of their nature, the levels of proinflammatory markers after the administration of nanomaterials were found to be significantly lower than those elicited by LPS injection at day 1 and day 2, when the LPS-induced upregulation was greatest. But an overall mild acute neuroinflammatory response was found for all the different nanomaterials tested, in comparison to the negative control. Although the administration of carbon NMs, including GO, elicited a mild upregulation of proinflammatory transcripts immediately after injection, still observable at day 2, gene expression levels for these materials were comparable to the negative control by day

7. These findings are in agreement with previous investigations in which f-MWNTs that were either carboxylated and aminated or aminated only, had been injected in the cerebral cortex of mice and induced in both cases a transient inflammatory reaction, attributed to both nanomaterial and brain surgery, with brain tissue showing no signs of inflammation by day 14.^[37] Contrastingly, injection of cationic liposomes induced marked levels of transcripts encoding proinflammatory markers (particularly at the site of injection) that persisted for up to 7 days after injection, in agreement with previous studies.^[48,49]

In brain regions close to (but not within) the injection site, there was an overall lower level of proinflammatory transcripts compared to the injection site. Apart from day 2, the administration of f-MWNTs and GO did not elicit upregulation of any proinflammatory mediators in a nearby brain region from the injection site, which is consistent with a previous study that did not reveal any diffusion of the biological effects after intracerebroventricular injection.^[37] However, despite the distance from the injection site, the administration of cationic liposomes induced marked upregulation of inflammatory markers in these brain regions at both day 1 and day 2. This suggests potential diffusion of either the biological response via intercellular signaling, possibly mediated by activated microglial cells, or the nanomaterials (or both). This observation is consistent with observations by Knudsen et al.^[48] In this study, macrophage infiltration was observed both in the injection site and in a nearby brain region 1 week after the injection of cationic and anionic liposomes in the dentate gyrus of rats.

Neurotoxicity leading to neurodegenerative effects represents a major concern for the use of nanocarriers in the brain.^[54] The results obtained in the present study did not reveal acute neuronal cell death effects for most of the analyzed nanomaterials. Indeed, cell counting revealed a significant decrease of neuronal cell number in the injection site only after administration of cationic liposomes. These findings are consistent with results obtained in a previous study in which the potential systemic and central toxic responses were evaluated after brain administration of non-PEGylated cationic (DOTAP:Chol-Chol) liposomes or PEGylated micelles that were either cationic or anionic.^[48] In the latter study, intracerebroventricular administration of cationic liposomes induced inflammatory cell infiltration, neuronal degeneration, and cell apoptosis, whereas the administration of anionic particles did not cause any toxic reaction.^[48] Similarly, in the present study, the DOPG:Chol anionic liposomes did not induce neurotoxicity, while cationic DOTAP:Chol liposomes resulted in neurotoxic effects. However, while LPS elicited glial and neuronal cell death at the site of injection, cationic liposomes only affected neuron cell number. This could be due to the properties of cationic liposomes, which are unstable nanosystems characterized by rapid clearance due to fusion with cell membranes, hence, are short-lived.^[64]

In contrast to liposomes, regardless of their surface charge none of the CNMs induced neurotoxicity. This is consistent with a previous long-term (12 weeks or 1 year) study on brain tissue response following the injection of nanowires with different lengths (2, 5, and 10 μm) in which no significant differences in the number of neurons were measured.^[59] In another study, PEGylated SWNTs did not induce cerebral tissue damage

or cognitive function alterations at 1 or 7 days after infusion in the rat hippocampus.^[39] In addition, despite short-term oxidative damage observed at 30 min, an unanticipated antioxidant effect was observed after 7 days, suggesting a potential neuroprotective ability of these functionalized carbon nanotubes.^[39]

The brain inflammatory response to nanocarrier injection is expected to be mediated by glial cells, since both microglia and astrocytes act as scavengers for maintaining homeostasis and signaling between cells. On one hand, astrocytes control ion and nutrient balance,^[65] and are activated upon injury, which manifests structurally by an hypertrophy of the cell body and processes, and an upregulation of GFAP.^[66] On the other hand, microglial cells are the main CNS immune-resident components, reacting to early changes in neuronal activity or to pathological conditions^[67] and constitute the main defense mechanism in the brain. Therefore, the responses of both microglial cells and astrocytes were analyzed in detail in the present study.

At the injection site, no activation of microglial cells was observed after injection of CNMs, regardless of their type or surface charge, whereas hypertrophic microglial cells were observed after injection of liposomes (also regardless of their surface charge). Interestingly, in the brain region adjacent to injection, mild microglia activation was observed after administration of both positively charged amino f-MWNTs and liposomes (anionic or cationic). These findings are consistent with a previous study in which a local inflammatory response was induced by f-MWNTs.^[37] In addition, a mild astrocyte response was observed here at the injection site 2 days after injection, particularly after administration of ox-MWNTs and anionic liposomes. In adjacent or distant brain regions, the astrocyte response was significantly lower with respect to the injection site. A previous *in vitro* study, performed on primary mixed glial cell cultures, emphasized the importance of microglial cells and how their number (with respect to other cells such as astrocytes) can affect biological outcomes.^[40] We observed that administration of cationic liposomes induced astrocyte activation at a distance from the injection site, consistent with the proinflammatory gene expression response observed in the same brain region with RT-qPCR analyses. These findings agree well with results obtained in a previous study in which both astrogliosis and microgliosis (based on GFAP and Iba1 immunostaining) were identified directly at the site of injection of cationic micelles or in nearby brain regions.^[48] In contrast, anionic micelles did not induce a similar activation, highlighting the safer profile of negatively charged nanomaterials when compared to positively charged nanomaterials. Indeed, anionic particles interact less with cell membranes that are negatively charged surface. In contrast, cationic particles, due to a higher electrostatic interaction with negatively charged cells, can accumulate to a greater extent in cells and create a more significant burden. This in turn increases the potential of positively charged nanomaterials to exert a toxic effect.^[68,69]

Regarding the overall brain inflammation potential of the different nanomaterials tested here, GO nanosheets appeared to have the least inflammatory profile, when combining both molecular and histological results. This is consistent with a recent review that mentioned that, thus far, graphene-based nanomaterials (including GO) appear to be safer than carbon nanotubes.^[70] When comparing carbon nanotubes and

carbon-based 2D lattices, not only the dimensions (lateral, thickness, or length) but also physicochemical features such as rigidity/stiffness or bioavailable surface area could be among the explanatory material factors making GO more tolerable than MWNTs under the tested conditions.^[71,72] However systematic investigations addressing those questions and comparing the two types of materials are lacking so far, in both the nanotoxicology and nanomedicine literatures. Here, we observed that GO nanosheets not only induced a moderate and acute inflammatory response (*tgf-β* overexpressed at day 1; *tnf-α* and *il-6* overexpressed at day 2; expression levels similar to negative control for all transcripts by day 7), but also led to a lower level of glial cell activation at day 2 when compared to vehicle injection (i.e., glial activation due solely to surgery in this later case), especially at the 1 mg mL⁻¹ dose. In addition, GO induced less neurotoxicity than LPS, cationic liposomes, or even the vehicle control. This suggests that the presence of GO in the brain could be beneficial to reduce the impact of intraparenchymal stereotactic surgical injection of materials, a traumatic injury that causes inflammation and cell death by itself, as evidenced in the negative control results reported here. These findings are consistent with a study^[50] that reported that mouse brain directly injected with GO had lower GFAP immunoreactivity at 48 h and lower *iba1* immunoreactivity at 72 h after injection compared to negative vehicle control, suggesting that GO had the capacity to lower the activation of astrocytes and microglial cells, both caused by the brain surgery at the injection site. In agreement with this, another study reported the immunomodulatory effects of GO pretreatment on the macrophage response to inflammatory challenge.^[45] In this study, GO pretreatment had an anti-inflammatory effect upon activation of the inflammasome. Specifically, GO sheets reduced the release of IL-1β and IL-6 by an NRF2-mediated mechanism. This effect was observed not only in immortalized bone marrow-derived macrophages but also in a primary murine mixed glia and immortalized microglia BV2 cell line. While all these converging findings, including ours, are encouraging from a biomedical perspective, they warrant further investigations to fully understand the underlying mechanism of the immunomodulatory effects of GO nanosheets. In particular a greater sample size, a broader range of doses and longer time points after injection will be required to reveal how these effects could be controlled and safely translated into valuable clinical applications of GO-based nanovectors for brain diseases.

4. Conclusion

In the present pilot study looking at the acute response to injection of nanovector candidates in the brain, lipid-based NPs, particularly cationic liposomes, induced the greatest inflammatory response in all considered brain regions. In contrast, CNMs were well-tolerated in the brain parenchyma, with assessments at both molecular and histological levels revealing only an acute response at day 1 and day 2 followed by fast recovery by day 7. No significant differences were observed between the two types of MWNT functionalization or the two doses of CNMs (1 μg vs 0.5 μg). Among the different CNMs, GO nanosheets displayed the least deleterious profile, with even some beneficial

immunomodulatory properties that mitigate the inherent inflammation and brain tissue damages associated with the brain stereotactic administration. Therefore, under the conditions tested here, GO nanosheets appeared to have the best profile for future development as brain nanovector, especially for cerebral applications that require focal drug administration or in conditions with an inherent inflammatory component. Going further, additional investigations should examine not only the long-term fate and chronic effects of these materials after their injection in the brain, but also the long-term consequences of the apparent immunomodulation properties of GO.

5. Experimental Section

Nanomaterials Production—Functionalized Multiwalled Carbon Nanotubes: Pristine MWNTs were purchased from Nanostructured and Amorphous Materials Inc. (NanoAmorph, Houston, TX, USA) with a carbon content of 94%. The pristine materials were then modified using either a 1,3-dipolar cycloaddition reaction to obtain aminated MWNTs (MWNT-NH₃⁺) or a 24 h reaction in H₂SO₄/HNO₃ (3:1) solution to produce carboxylated MWNTs (ox-MWNT), as previously described.^[73,74]

Nanomaterials Production—Graphene Oxide Sheets: GO flake suspensions in water were prepared from graphite powder (Merck, Sigma-Aldrich, UK) and synthesis was conducted using a modified Hummers' method as previously described.^[56,57]

Nanomaterials Production—Liposomes: To produce liposomes, DOTAP and DOPG were kindly provided by Lipoid GmbH (Ludwigshafen, Germany). Chol was purchased from Merck Sigma-Aldrich (UK). Chloroform and methanol were purchased from Thermo Fisher Scientific (UK). Both cationic (DOTAP/Chol; 2 × 10⁻³ M DOTAP:1 × 10⁻³ M Chol) and anionic (DOPG/Chol; 2 × 10⁻³ M DOPG:1 × 10⁻³ M Chol) liposomes were prepared using the film hydration method.^[75] Briefly, DOTAP or DOPG and Chol were dissolved in chloroform/methanol (4:1, v/v) and the organic solvents were evaporated under pressure for 30 min at +40 °C using a rotary evaporator. The resulting thin lipid film was hydrated in sterile-filtered 5% (w/v) dextrose solution in water and then bath sonicated for 15 min at +40 °C. The final liposome solution was kept at room temperature for 30 min to stabilize the colloidal stability before storage at +4 °C for a maximum of 5 days.

Characterization of the Nanomaterials—Functionalized Multiwalled Carbon Nanotubes: MWNTs were analyzed by TEM to determine the mean diameter and length as previously described for the aminated and carboxylated MWNTs.^[37,74] A Kaiser test was used for MWNT-NH₃⁺ to measure the amount of amine functionalization as previously reported.^[73] Kaiser test is based on the colorimetric reaction between the ninhydrin reagent and the amine groups. The reaction gives a blue color readout and the intensity is proportionally related to the amount of free terminal amine groups.^[76] Dynamic light scattering (DLS) was not used to assess hydrodynamic diameter of the MWNTs sheets, as it has been proven nonreliable for 1D tube-shaped materials. More systemic characterization of these materials had been previously reported.

Characterization of the Nanomaterials—Graphene Oxide Sheets: GO sheets were characterized by several techniques, including electrophoretic mobility (Nano Zeta Sizer ZS, ZEN3600, Malvern Panalytical, Malvern, UK), TEM (Philips/FEI, Thermo Fisher Scientific, UK), and AFM (Bruker, UK) to assess physicochemical properties. These properties include ζ-potential, lateral dimensions, and the thickness of the sheets. For electrophoretic mobility measurements, dispersions were placed into U-shaped cuvettes equipped with gold electrodes. The ζ-potential is related to the electrophoretic mobility by Henry's equation valid in the Smoluchowski approximation, when the screening length is much smaller than the particle radius. DLS was not used to assess hydrodynamic diameter of the GO sheets, as it has been proven nonreliable for 2D plate-shaped materials. More systemic

characterization of these materials were reported previously^[57] (in this reference, the GO sheets used herein are named small GO).

Characterization of the Nanomaterials—Liposomes: Liposomes were first characterized by the DLS technique. Particle diameter and electrophoretic mobility of cationic and anionic liposomes were measured at 25 ± 0.1 °C using a Zeta-Sizer unit (Nano Zeta Sizer ZS, ZEN3600, Malvern Panalytical, Malvern, UK). The particle size was based on DLS in back-scattering mode, at 173° and excitation $\lambda = 632.8$ nm. The prepared liposomes were also analyzed using TEM (Philips/FEI, Thermo Fisher Scientific, UK).

Preparation of Nanomaterials for Brain Injection—Functionalized Multiwalled Carbon Nanotubes: The day before injection, dry powders of MWNT-NH₃⁺ and ox-MWNT were weighed, exposed to low energy UV light for 6 h in order to “sterilize” the nanotubes, and then rehydrated with sterile-filtered 5% dextrose solution in water (final concentration 1 mg mL⁻¹) in sterilized glass container. This material suspension was initially sonicated for 45 min using a water bath sonicator (VWR, UK) operating at 80 W (45 kHz) to allow dispersion of the nanotubes in the dextrose solution. A 0.5 mg mL⁻¹ suspension was achieved by further dilution in sterile-filtered 5% dextrose solution. All colloidal suspensions kept at +4 °C were sonicated for an additional 15 min immediately before the injection.

Preparation of Nanomaterials for Brain Injection—Graphene Oxide Sheets: Dry powder of GO sheets that were exposed to UV light for 6 h after weighting was also rehydrated in sterile-filtered 5% dextrose solution at a concentration of 1 mg mL⁻¹. This suspension was sonicated for 30 min using a water bath sonicator (VWR, UK) operating at 80 W (45 kHz) to allow dispersion of GO flakes in the dextrose solution. The 0.5 mg mL⁻¹ suspension used here was achieved by further dilution in sterile-filtered 5% dextrose solution.

Preparation of Nanomaterials for Brain Injection—Liposomes: Liposomes were initially prepared at 2×10^{-3} M DOTAP: 1×10^{-3} M Chol or 2×10^{-3} M DOPG: 1×10^{-3} M Chol and then further diluted to the final concentration of 1 mg mL⁻¹ in sterile-filtered 5% dextrose solution.

The vehicle used for all nanomaterials, sterile-filtered 5% dextrose solution, was used as negative control (i.e., basic conditions of inflammation following stereotactic injection of an isotonic solution, such as 5% dextrose in water). LPS O111:B4 suspension at 5 mg mL⁻¹ in sterile-filtered 5% dextrose solution was used as positive control for inflammatory reaction.^[37]

Animals and Sample Preparation: A total of 84 young (3 week old) C57BL/6 male mice were used. The protocol received ethical approval from the University of Manchester under authorization from the United Kingdom Home Office (project License number PPL-70/7763). Suffering was minimized and the minimal number of animals were used in accordance with the Code of Practice for the housing and care of animals used in scientific procedures. The animals were kept in groups of four to five in standard cages with free access to food and water under controlled environmental conditions, including a 12 h/12 h light/dark cycle.

For surgery, mice were initially anesthetized with isoflurane inhalation, injected with analgesic (buprenorphine 0.1 mg kg⁻¹, im), and then placed on a stereotactic apparatus. A hole was drilled in the skull at specific lateral coordinates. A total of 1 µL of the different nanomaterials suspended in 5% dextrose in water was injected in the striatum with a microsyringe mounted on a stereotaxic holder (coordinates used: lateral (x) -0.1 mm, ventral (y) -2.3 mm, and rostro-caudal (z) -3.0 mm from bregma).^[77]

During the surgical procedure, the mice were kept under oxygen and heated using a blanket with a thermostat to maintain body temperature at ≈37 °C. At the end of the procedure, the wound was sutured and the animal was maintained in a thermally controlled incubation chamber at 37 °C until complete recovery from anesthesia. The mice were then returned to their maintenance cages and culled at different time points as shown in the experimental design (Figure 1A).

Mice used for gene expression analyses were sacrificed at 1, 2, or 7 days after injection ($n = 3$ per group; total of 63 mice). They were culled with CO₂ exposure followed by cerebral dislocation. The brain was

then rapidly dissected out and cut into 2 mm thick slices using a Zivic stainless brain slicer matrix. For each brain, four coronal slices were prepared: one containing the injected area, one immediately posterior to assess diffusion of nanomaterials or of signal in a region adjacent to the injection, and two anterior to the injected area. The most anterior of the latter two slices was used to assess diffusion of nanomaterials or of signal in a distant brain region. From the three brain slices thus sampled, a $2 \times 2 \times 2$ mm tissue block was dissected for RT-qPCR analysis (Figure 1A). In the slice containing the injection site, the sampled tissue block was centered on this site. In the adjacent posterior slice and in the anterior slice, the tissue blocks were sampled along the same antero-posterior and dorso-ventral axes of the injection site. The tissue blocks were snap-frozen in liquid nitrogen and cryopreserved for RNA extraction and real-time RT-qPCR analysis.

Animals for colorimetric histochemical and immunohistochemical procedures were sacrificed at day 2 after injection ($n = 3$ per group; total of 21 mice). They were anaesthetized by isoflurane inhalation and then cardiac-perfused with 4% paraformaldehyde in 0.01 M phosphate-buffered saline (PBS), pH 7.4. The brain was then dissected out and immersed overnight in 4% paraformaldehyde in PBS. The following day, brains were soaked in sucrose (5%, 15%, and 30% steps) at 4 °C for cryoprotection following a previously described procedure.^[37]

Real-Time Quantitative PCR Analysis: Tissue blocks from animals injected with GO (0.5 mg mL⁻¹), MWNT-NH₃⁺ (0.5 mg mL⁻¹), ox-MWNT (0.5 mg mL⁻¹), cationic liposomes (1 mg mL⁻¹), anionic liposomes (1 mg mL⁻¹), 5% dextrose (vehicle, negative control), or LPS (positive control) were used for transcript analysis. Tissue blocks were homogenized with a TissueLyser LT (Qiagen, The Netherlands) and total RNA was extracted using a NucleoSpin RNA/Protein kit (Macherey-Nagel, Germany) according to the manufacturer's instructions. The concentration of RNA was determined as the optical density ratio 260 nm/280 nm using a BioPhotometer plus (Eppendorf, Germany). Ratio values between 1.8 and 2.2 were considered good quality. Samples of cDNA were prepared from 1 mg RNA in a total volume of 20 µL using the BioRad iScript cDNA Synthesis Kit (BioRad, USA). Samples were run on a CFX-96 Real Time Detection System (BioRad, USA) with the following sequence: 95 °C for 3 min (initial denaturation step), 1 cycle; 95 °C for 10 s (amplification), 60 °C for 30 s (annealing), repeated for 40 cycles. Amplification was followed by a melting-curve analysis to confirm PCR product specificity.

Each RT-PCR reaction in a 25 µL total volume contained 2 µL of cDNA from reverse transcription PCR, 12.5 µL Fast SYBR Green Master Mix (BioRad, UK), and primers at 200×10^{-9} M each (Merck-Sigma-Aldrich, UK; see Table S1 in the Supporting Information for reverse and forward primer sequences). Gene expression levels (*tnf-α*, *il-1β*, *il-6*, *il-12*, *ifn-γ*, *cxcl10*, *ccl2*, *il-10*, *tgf-β*, *il-4*, and housekeeping gene *β-actin*) were calculated using the Livak method, based on calculation of $2^{-\Delta\Delta CT}$.^[78] *β-actin* was used as a reference housekeeping gene to normalize the amount of target primer transcripts. The normalized values for each gene were compared to the relative expression for 5% dextrose (negative control) to calculate the fold increase of the target gene in the sample.

Immunohistochemical and Histochemical Procedures—Tissue Processing: Brains (day 2 postinjection) from animals injected with GO (0.5 and 1 mg mL⁻¹), MWNT-NH₃⁺ (0.5 and 1 mg mL⁻¹), ox-MWNT (0.5 and 1 mg mL⁻¹), cationic liposomes (1 mg mL⁻¹), anionic liposomes (1 mg mL⁻¹), 5% dextrose (vehicle, negative control), or LPS (positive control) were used for cell analyses.

Following cardiac perfusion of fixative under anesthesia (as described above), postfixation, and brain cryoprotection in sucrose, brains were snap-frozen and then cut using a cryo-microtome into 30 µm thick serial coronal sections. Series of sections (one every 360 µm) were collected in the following three regions: i) anterior to the injection site (from +1.9 to +1.0 from bregma), ii) at the injection site (from -0.1 to -0.9 from bregma), and iii) posterior to it (from -1.2 to -2.0 from bregma).

Immunohistochemical and Histochemical Procedures—Immunophenotyping of Neurons, Microglia, Astrocytes, and Apoptotic Cells: For each experimental group ($n = 3$ animals per group), a series of sections was processed for immunohistochemistry. Free-floating sections were pretreated with 1% H₂O₂ (Merck Sigma-Aldrich, UK) for

15 s at room temperature, rinsed in PBS (Merck Sigma-Aldrich, UK), and incubated in 5% normal serum of the appropriate species (Vector Lab, USA; Table S2, Supporting Information), and 0.03% Triton-X100 (Merck Sigma-Aldrich, UK) in PBS for 1 h at room temperature to prevent nonspecific binding. After rinsing in PBS, the sections were incubated overnight at 4 °C in primary antibodies (Table S2, Supporting Information) diluted in 1% normal serum in PBS. The sections were then incubated in biotinylated secondary antibodies (Vector Lab) in 1% normal serum in PBS. The sections were then reacted with the Vectastain ABC kit (Vector Lab) and finally with 0.5% 3-3' diaminobenzidine (DAB, Merck-Sigma-Aldrich) in PBS. After rinsing, the sections were dehydrated through an increasing alcohol gradient, mounted, and cover-slipped. The sections were examined with an Olympus microscope equipped with a QICAM digital camera (QImaging, Canada) using Image-Pro Plus 7.0 Software (Media Cybernetics, USA).

Immunohistochemical and Histochemical Procedures—Fluoro-Jade B Histochemistry: To evaluate ongoing neuronal cell death, Fluoro-Jade B staining was performed.^[60] Sections were mounted on gelatin-coated slides, air dried, and soaked for 5 min in 1% NaOH (Merck-Sigma-Aldrich) in 80% alcohol in distilled water. The sections were then soaked for 2 min in 70% alcohol and 2 min in distilled water, and then in a solution of 0.06% potassium permanganate (Merck Sigma-Aldrich) for 10 min to reduce the background signal. The sections were then rinsed in distilled water for 2 min and soaked for 15 min in the staining solution. The Fluoro-Jade B working solution (0.0004%) was obtained by diluting 4 mL of 0.01% stock solution (10 mg of powder (Histochem Inc., USA) in 100 mL of distilled water) into 96 mL of 0.1% acetic acid (Merck Sigma-Aldrich). The sections were then rinsed in distilled water and air dried. They were cleared in xylene for 2 min, mounted, and then cover-slipped. The sections were analyzed with an Olympus microscope equipped with a UV bulb light source (450–490 nm blue excitation light filter; Fluoro-Jade B has a green light emission) and images were taken with a QICAM digital camera (QImaging, Surrey, BC, Canada).

Quantitative Analyses—Counts of Neurons and Astrocytes: To assess whether the intrastriatal injection of nanomaterials induced neuronal cell loss, the number of neurons identified by NeuN immunoreactivity was estimated using a stereological approach in all groups of mice (animals sacrificed at day 2 after injection of all the materials; $n = 3$ per group; total of 21 mice).

Stereology was also used to estimate the number of astrocytes. This was based on GFAP immunostaining in the mice treated with 5% dextrose, LPS, or cationic liposomes. Cell counting was performed using three regions of interest (ROIs) per section in six sections (2 regularly spaced sections through the anterior region, the injection site, and the posterior region, respectively) per mouse and three mice per group. The counting of astrocytes was performed in three ROIs per section in six sections sampled as above per mouse and three mice per group. Sections were analyzed with an Olympus microscope equipped with a Retiga-2000R CCD Camera (QImaging, Canada) and counting was performed with the Optical Fractionator probe included in Stereo Investigator 10 software (MBF Bioscience, USA).

Quantitative Analyses—Analysis of Glial Cell Coverage and Optical Density of Microglial Cells: A series of sections for each condition ($n = 3$; immunostained as described above for visualization of microglial cells and astrocytes) were used to assess the percentage of the area covered by CD11b- and GFAP-immunopositive cells, assuming that a larger area is covered by activated glial cells than by “resting” cells.^[79,80] The immunostaining was thus quantified as the percentage of the total image area, considering the site of injection in the striatum and an equivalent ROI in the anterior and posterior sections.

The intensity of the CD11b immunoreactivity was also quantified by densitometry. A quantitative densitometric analysis^[81–83] was performed to measure (in the same sections) the intensity of immunoreactivity signal in the cell somata.^[84] For this analysis, three ROIs (with an area of 289 μm^2) per section in six sections per mouse sampled as above and in three mice per group were used. Sections were analyzed with an Olympus microscope and 8-bit grey-scale images were taken with a 20 \times objective and a QImaging QICAM digital camera (QImaging,

Canada) maintaining constant light conditions and magnification. Images were then processed using the Image-Pro Plus 7.0 software (Media Cybernetics, USA). A signal from nonimmunostained tissue (contralateral hemisphere) was used to subtract the background signal.

Statistics: The results were expressed as mean per group \pm standard error of the mean (SEM). The Livak method was used to analyze qPCR data using ΔCT values.^[78] Data were checked for normal distribution before running statistical analysis. Statistical variations were evaluated as follows: for simple comparisons unpaired t -tests were used and one-way analysis of variance (ANOVA) per group, followed by Bonferroni post-hoc for testing pairwise comparisons. For immunohistochemical and histochemical analysis, the number of sample units used in each study group ($n = 3$) was compensated by different measures of the parameter (3 different ROIs) in the areas of interest, within the brain (anterior site, injection site, and posterior site). GraphPad Prism (GraphPad Software v.6) was used for statistical analyses. p -values < 0.05 were considered significant.

Supporting Information

Supporting Information is available from the Wiley Online Library or from the author.

Acknowledgements

The authors would like to thank Dr. Irene de Lázaro for fruitful discussion regarding statistical analyses of the RT-qPCR data, Lana Papafilippou for the TEM imaging of the cationic liposomes, and Dr. Marco Sandri (Big and Open Data Innovation Laboratory - BODal-Lab, University of Brescia, Italy) for the valuable scientific support in the biostatistical analysis of the data. Graphical abstract and Figure 1A were created using BioRender.com. This work was partly supported by the EU H2020 RTD Framework Program: FET Graphene Flagship project (GrapheneCore3, Grant agreement ID: 881603), the Centre National de la Recherche Scientifique (CNRS), the International Center for Frontier Research in Chemistry (icFRC), and the Agence Nationale de la Recherche (ANR) through the LabEx project Chemistry of Complex Systems (ANR-10-LABX-0026_CSC). M.P., as the recipient of the AXA Carbon Bionanotechnology Chair, is grateful to the AXA Research Fund for financial support. MP was also supported by the Spanish Ministry of Economy and Competitiveness MINECO (project CTQ2016-76721-R), the University of Trieste, and the Spanish State Research Agency (Maria de Maeztu Units of Excellence Program Grant No. MDM-2017-0720). Financial support to this project was partially provided by the Fondazione Cariverona (“Verona Nanomedicine Initiative”) and funding from an intramural (University of Verona) international cooperation program (“CooperInt”) was obtained. K.K. would like to acknowledge the Severo Ochoa Centre of Excellence Award to ICN2.

Conflict of Interest

The authors declare no conflict of interest.

Author Contributions

C.P., C.B., and K.K. conceived the overall design of the project with contributions from A.B and M.P. to the planning of the experiments. C.P. and C.B. implemented the experiments and analyzed the data under the supervision of C.B., K.K., and M.B., with contributions from M.M., D.A.J., and N.L. D.A.J. prepared the GO sheets and N.L. prepared the liposomes. A.B. and M.P. produced and characterized the functionalised carbon nanotubes. C.P. and C.B. wrote the manuscript

draft. All authors discussed the results, contributed to the writing and critical revision of the article, and approved the version to be published.

Data Availability

The raw/processed data required to reproduce these findings cannot be shared at this time as the data also forms part of an ongoing study.

Keywords

biocompatibility, brain, carbon nanotubes, graphene, immunomodulation, inflammation, liposomes

Received: July 3, 2020

Revised: October 9, 2020

Published online: November 10, 2020

- [1] D. Furtado, M. Bjornmalm, S. Ayton, A. I. Bush, K. Kempe, F. Caruso, *Adv. Mater.* **2018**, *30*, 1801362.
- [2] Y. Cheng, R. A. Morshed, B. Auffinger, A. L. Tobias, M. S. Lesniak, *Adv. Drug Delivery Rev.* **2014**, *66*, 42.
- [3] L. Biddlestone-Thorpe, N. Marchi, K. Guo, C. Ghosh, D. Janigro, K. Valerie, H. Yang, *Adv. Drug Delivery Rev.* **2012**, *64*, 605.
- [4] A. Dominguez, B. Suarez-Merino, F. Goni-de-Cerio, *J. Nanosci. Nanotechnol.* **2014**, *14*, 766.
- [5] G. Modi, V. Pillay, Y. E. Choonara, V. M. Ndesendo, L. C. du Toit, D. Naidoo, *Prog. Neurobiol.* **2009**, *88*, 272.
- [6] M. Caffo, L. Merlo, D. Marino, G. Caruso, *Nanomedicine* **2015**, *10*, 615.
- [7] J. T. Wang, K. T. Al-Jamal, *Nanomedicine* **2015**, *10*, 2639.
- [8] H. Kafa, J. T. Wang, K. T. Al-Jamal, *Int. Rev. Neurobiol.* **2016**, *130*, 229.
- [9] B. S. Wong, S. L. Yoong, A. Jagusiak, T. Panczyk, H. K. Ho, W. H. Ang, G. Pastorin, *Adv. Drug Delivery Rev.* **2013**, *65*, 1964.
- [10] M. Bramini, G. Alberini, E. Colombo, M. Chiacchiaretta, M. L. DiFrancesco, J. F. Maya-Vetencourt, L. Maragliano, F. Benfenati, *Front. Syst. Neurosci.* **2018**, *12*, 12.
- [11] A. Bianco, K. Kostarelos, C. D. Partidos, M. Prato, *Chem. Commun.* **2005**, *5*, 571.
- [12] A. Bianco, K. Kostarelos, M. Prato, *Curr. Opin. Chem. Biol.* **2005**, *9*, 674.
- [13] L. Lacerda, A. Bianco, M. Prato, K. Kostarelos, *Adv. Drug Delivery Rev.* **2006**, *58*, 1460.
- [14] K. Kostarelos, K. S. Novoselov, *Nat. Nanotechnol.* **2014**, *9*, 744.
- [15] T. A. Mattei, *Expert Rev. Neurother.* **2014**, *14*, 845.
- [16] X. Guo, N. Mei, *J. Food Drug Anal.* **2014**, *22*, 105.
- [17] K. Zhou, G. A. Thouas, C. C. Bernard, D. R. Nisbet, D. I. Finkelstein, D. Li, J. S. Forsythe, *ACS Appl. Mater. Interfaces* **2012**, *4*, 4524.
- [18] S. M. Chowdhury, C. Surhland, Z. Sanchez, P. Chaudhary, M. A. Suresh Kumar, S. Lee, L. A. Pena, M. Waring, B. Sitharaman, M. Naidu, *Nanomedicine* **2015**, *11*, 109.
- [19] J. Ren, S. Shen, D. Wang, Z. Xi, L. Guo, Z. Pang, Y. Qian, X. Sun, X. Jiang, *Biomaterials* **2012**, *33*, 3324.
- [20] M. K. Gottipati, E. Bekyarova, R. C. Haddon, V. Parpura, *Amino Acids* **2015**, *47*, 1379.
- [21] X. Xue, L. R. Wang, Y. Sato, Y. Jiang, M. Berg, D. S. Yang, R. A. Nixon, X. J. Liang, *Nano Lett.* **2014**, *14*, 5110.
- [22] K. T. Al-Jamal, L. Gherardini, G. Bardi, A. Nunes, C. Guo, C. Bussy, M. A. Herrero, A. Bianco, M. Prato, K. Kostarelos, T. Pizzorusso, *Proc. Natl. Acad. Sci. USA* **2011**, *108*, 10952.
- [23] Z. Yang, Y. Zhang, Y. Yang, L. Sun, D. Han, H. Li, C. Wang, *Nanomedicine* **2010**, *6*, 427.
- [24] H. Kafa, J. T. Wang, N. Rubio, K. Venner, G. Anderson, E. Pach, B. Ballesteros, J. E. Preston, N. J. Abbott, K. T. Al-Jamal, *Biomaterials* **2015**, *53*, 437.
- [25] S. Shityakov, E. Salvador, G. Pastorin, C. Forster, *Int. J. Nanomed.* **2015**, *10*, 1703.
- [26] H. Kafa, J. T. Wang, N. Rubio, R. Klippstein, P. M. Costa, H. A. Hassan, J. K. Sosabowski, S. S. Bansal, J. E. Preston, N. J. Abbott, K. T. Al-Jamal, *J. Controlled Release* **2016**, *225*, 217.
- [27] J. T. Wang, N. Rubio, H. Kafa, E. Venturelli, C. Fabbro, C. Menard-Moyon, T. Da Ros, J. K. Sosabowski, A. D. Lawson, M. K. Robinson, M. Prato, A. Bianco, F. Festy, J. E. Preston, K. Kostarelos, K. T. Al-Jamal, *J. Controlled Release* **2016**, *224*, 22.
- [28] Y. Liu, L. P. Xu, W. Dai, H. Dong, Y. Wen, X. Zhang, *Nanoscale* **2015**, *7*, 19060.
- [29] M. Li, X. Yang, J. Ren, K. Qu, X. Qu, *Adv. Mater.* **2012**, *24*, 1722.
- [30] L. Feng, L. Wu, X. Qu, *Adv. Mater.* **2013**, *25*, 168.
- [31] G. Liu, H. Shen, J. Mao, L. Zhang, Z. Jiang, T. Sun, Q. Lan, Z. Zhang, *ACS Appl. Mater. Interfaces* **2013**, *5*, 6909.
- [32] Y. Kang, J. Liu, S. Yin, Y. Jiang, X. Feng, J. Wu, Y. Zhang, A. Chen, Y. Zhang, L. Shao, *ACS Nano* **2020**, *14*, 3059.
- [33] H. Peluffo, U. Unzueta, M. L. Negro-Demontel, Z. Xu, E. Vaquez, N. Ferrer-Miralles, A. Villaverde, *Biotechnol. Adv.* **2015**, *33*, 277.
- [34] M. W. Salter, B. Stevens, *Nat. Med.* **2017**, *23*, 1018.
- [35] M. Bentivoglio, R. Mariotti, G. Bertini, *Brain Res. Rev.* **2011**, *66*, 152.
- [36] G. Bardi, P. Tognini, G. Ciofani, V. Raffa, M. Costa, T. Pizzorusso, *Nanomedicine* **2009**, *5*, 96.
- [37] G. Bardi, A. Nunes, L. Gherardini, K. Bates, K. T. Al-Jamal, C. Gaillard, M. Prato, A. Bianco, T. Pizzorusso, K. Kostarelos, *PLoS One* **2013**, *8*, e80964.
- [38] L. Dal Bosco, G. E. Weber, G. M. Parfitt, K. Paese, C. O. Goncalves, T. M. Serodre, C. A. Furtado, A. P. Santos, J. M. Monserrat, D. M. Barros, *Biomed. Res. Int.* **2015**, *2015*, 104135.
- [39] L. Dal Bosco, G. E. Weber, G. M. Parfitt, A. P. Cordeiro, S. K. Sahoo, C. Fantini, M. C. Klosterhoff, L. A. Romano, C. A. Furtado, A. P. Santos, J. M. Monserrat, D. M. Barros, *PLoS One* **2015**, *10*, e0129156.
- [40] C. Bussy, K. T. Al-Jamal, J. Boczkowski, S. Lanone, M. Prato, A. Bianco, K. Kostarelos, *ACS Nano* **2015**, *9*, 7815.
- [41] L. Yang, F. Wang, H. Han, L. Yang, G. Zhang, Z. Fan, *Colloids Surf., B* **2015**, *129*, 21.
- [42] R. Rauti, N. Lozano, V. Leon, D. Scaini, M. Musto, I. Rago, F. P. Ulloa Severino, A. Fabbro, L. Casalis, E. Vazquez, K. Kostarelos, M. Prato, L. Ballerini, *ACS Nano* **2016**, *10*, 4459.
- [43] M. Bramini, S. Sacchetti, A. Armirotti, A. Rocchi, E. Vazquez, V. L. Castellanos, T. Bandiera, F. Cesca, F. Benfenati, *ACS Nano* **2016**, *10*, 7154.
- [44] M. Chiacchiaretta, M. Bramini, A. Rocchi, A. Armirotti, E. Giordano, E. Vazquez, T. Bandiera, S. Ferroni, F. Cesca, F. Benfenati, *Nano Lett.* **2018**, *18*, 5827.
- [45] C. Hoyle, J. Rivers-Auty, E. Lemarchand, S. Vranic, E. Wang, M. Buggio, N. J. Rothwell, S. M. Allan, K. Kostarelos, D. Brough, *ACS Nano* **2018**, *12*, 11949.
- [46] H. Lv, S. Zhang, B. Wang, S. Cui, J. Yan, *J. Controlled Release* **2006**, *114*, 100.
- [47] M. C. Filion, N. C. Phillips, *Biochim. Biophys. Acta* **1997**, *1329*, 345.
- [48] K. B. Knudsen, H. Northeved, P. K. Ek, A. Permin, T. L. Andresen, S. Larsen, K. M. Wegener, H. R. Lam, J. Lykkesfeldt, *Nanotoxicology* **2014**, *8*, 764.
- [49] K. B. Knudsen, H. Northeved, P. E. Kumar, A. Permin, T. Gjetting, T. L. Andresen, S. Larsen, K. M. Wegener, J. Lykkesfeldt, K. Jantzen, S. Loft, P. Moller, M. Roursgaard, *Nanomedicine* **2015**, *11*, 467.
- [50] R. Rauti, M. Medelin, L. Newman, S. Vranic, G. Reina, A. Bianco, M. Prato, K. Kostarelos, L. Ballerini, *Nano Lett.* **2019**, *19*, 2858.

- [51] C. Klumpp, K. Kostarelos, M. Prato, A. Bianco, *Biochim. Biophys. Acta* **2006**, 1758, 404.
- [52] A. Bianco, K. Kostarelos, M. Prato, *Chem. Commun.* **2011**, 47, 10182.
- [53] A. Nunes, C. Bussy, L. Gherardini, M. Meneghetti, M. A. Herrero, A. Bianco, M. Prato, T. Pizzorusso, K. T. Al-Jamal, K. Kostarelos, *Nanomedicine* **2012**, 7, 1485.
- [54] A. Nunes, K. Al-Jamal, T. Nakajima, M. Hariz, K. Kostarelos, *Arch. Toxicol.* **2012**, 86, 1009.
- [55] C. Bussy, C. Hadad, M. Prato, A. Bianco, K. Kostarelos, *Nanoscale* **2016**, 8, 590.
- [56] A. D. Jasim, N. Lozano, K. Kostarelos, *2D Mater.* **2016**, 3, 014006.
- [57] A. F. Rodrigues, L. Newman, N. Lozano, S. P. Mukherjee, B. Fadeel, C. Bussy, K. Kostarelos, *2D Mater.* **2018**, 5, 035020.
- [58] C. Mamot, J. B. Nguyen, M. Pourdehnad, P. Hadaczek, R. Saito, J. R. Bringas, D. C. Drummond, K. Hong, D. B. Kirpotin, T. McKnight, M. S. Berger, J. W. Park, K. S. Bankiewicz, *J. Neuro-Oncol.* **2004**, 68, 1.
- [59] L. Gallentoft, L. M. Pettersson, N. Danielsen, J. Schouenborg, C. N. Prinz, C. E. Linsmeier, *Biomaterials* **2015**, 42, 172.
- [60] L. C. Schmued, K. J. Hopkins, *Brain Res.* **2000**, 874, 123.
- [61] V. Mirshafiee, W. Jiang, B. Sun, X. Wang, T. Xia, *Mol. Ther.* **2017**, 25, 1522.
- [62] C. J. Bullock, C. Bussy, *Adv. Mater. Interfaces* **2019**, 6, 1900229.
- [63] P. Møller, J. Lykkesfeldt, *Nanomedicine* **2014**, 9, 1441.
- [64] M. L. Immordino, F. Dosio, L. Cattel, *Int. J. Nanomed.* **2006**, 1, 297.
- [65] M. Simard, M. Nedergaard, *Neuroscience* **2004**, 129, 877.
- [66] M. V. Sofroniew, H. V. Vinters, *Acta Neuropathol.* **2010**, 119, 7.
- [67] M. L. Block, L. Zecca, J. S. Hong, *Nat. Rev. Neurosci.* **2007**, 8, 57.
- [68] S. J. Soenen, E. Illyes, D. Vercauteren, K. Braeckmans, Z. Majer, S. C. De Smedt, M. De Cuyper, *Biomaterials* **2009**, 30, 6803.
- [69] R. Banerjee, *J. Biomater. Appl.* **2001**, 16, 3.
- [70] B. Fadeel, C. Bussy, S. Merino, E. Vazquez, E. Flahaut, F. Mouchet, L. Evariste, L. Gauthier, A. J. Koivisto, U. Vogel, C. Martin, L. G. Delogu, T. Buerki-Thurnherr, P. Wick, D. Beloin-Saint-Pierre, R. Hirschier, M. Pelin, F. Candotto Carniel, M. Tretiach, F. Cesca, F. Benfenati, D. Scaini, L. Ballerini, K. Kostarelos, M. Prato, A. Bianco, *ACS Nano* **2018**, 12, 10582.
- [71] C. Bussy, H. Ali-Boucetta, K. Kostarelos, *Acc. Chem. Res.* **2013**, 46, 692.
- [72] M. Rezazadeh Azari, Y. Mohammadian, *Environ. Sci. Pollut. Res. Int.* **2020**, 27, 15401.
- [73] V. Georgakilas, N. Tagmatarchis, D. Pantarotto, A. Bianco, J. P. Briand, M. Prato, *Chem. Commun.* **2002**, 3050.
- [74] S. Li, W. Wu, S. Campidelli, V. Sarnatskaia, M. Prato, A. Tridon, A. Nikolaev, V. Nikolaev, A. Bianco, E. Snezhkova, *Carbon* **2008**, 46, 1091.
- [75] N. Lozano, W. T. Al-Jamal, A. Taruttis, N. Beziere, N. C. Burton, J. Van den Bossche, M. Mazza, E. Herzog, V. Ntziachristos, K. Kostarelos, *J. Am. Chem. Soc.* **2012**, 134, 13256.
- [76] E. Kaiser, R. L. Colescott, C. D. Bossinger, P. I. Cook, *Anal. Biochem.* **1970**, 34, 595.
- [77] G. Paxinos, K. Franklin, *Paxinos and Franklin's the Mouse Brain in Stereotaxic Coordinates*, Academic Press, San Diego, CA **2012**.
- [78] K. J. Livak, T. D. Schmittgen, *Methods* **2001**, 25, 402.
- [79] H. Dou, K. Birusingh, J. Faraci, S. Gorantla, L. Y. Poluektova, S. B. Maggirwar, S. Dewhurst, H. A. Gelbard, H. E. Gendelman, *J. Neurosci.* **2003**, 23, 9162.
- [80] H. Dou, J. Morehead, J. Bradley, S. Gorantla, B. Ellison, J. Kingsley, L. M. Smith, W. Chao, G. Bentsman, D. J. Volsky, H. E. Gendelman, *Glia* **2006**, 54, 81.
- [81] A. C. Ferraz, L. L. Xavier, S. Hernandez, M. Sulzbach, G. G. Viola, J. A. Anselmo-Franci, M. Achaval, C. D. Cunha, *Brain Res.* **2003**, 986, 200.
- [82] L. L. Xavier, G. G. Viola, A. C. Ferraz, C. D. Cunha, J. M. Deonizio, C. A. Netto, M. Achaval, *Brain Res. Protoc.* **2005**, 16, 58.
- [83] F. G. Martinez, E. E. Hermel, L. L. Xavier, G. G. Viola, J. Riboldi, A. A. Rasia-Filho, M. Achaval, *Brain Res.* **2006**, 1108, 117.
- [84] L. Saur, P. P. Baptista, P. N. de Senna, M. F. Paim, P. do Nascimento, J. Ilha, P. B. Bagatini, M. Achaval, L. L. Xavier, *Brain Struct. Funct.* **2014**, 219, 293.